Geosci. Model Dev. Discuss., 6, 4105–4136, 2013
www.geosci-model-dev-discuss.net/6/4105/2013/
doi:10.5194/gmdd-6-4105-2013

Geoscientific Model Development Discussions
Open Access

Equivalent sensor radiance generation and remote sensing from model parameters – Part 1: Equivalent sensor radiance formulation

G. Wind[1,2], A. M. da Silva[1], P. M. Norris[1,3], and S. Platnick[1]

[1]NASA Goddard Space Flight Center, 8800 Greenbelt Rd. Greenbelt, Maryland, 20771, USA
[2]SSAI, Inc. 10210 Greenbelt Road, Suite 600, Lanham, Maryland 20706, USA
[3]Universities Space Research Association, 10211 Wincopin Circle #500, Columbia, MD 21044, USA

Received: 19 June 2013 – Accepted: 12 July 2013 – Published: 26 July 2013

Correspondence to: G. Wind (gala.wind@nasa.gov)

Published by Copernicus Publications on behalf of the European Geosciences Union.

Abstract

In this paper we describe a general procedure for calculating equivalent sensor radiances from variables output from a global atmospheric forecast model. In order to take proper account of the discrepancies between model resolution and sensor footprint the algorithm takes explicit account of the model subgrid variability, in particular its description of the probability density function of total water (vapor and cloud condensate). The equivalent sensor radiances are then substituted into an operational remote sensing algorithm processing chain to produce a variety of remote sensing products that would normally be produced from actual sensor output. This output can then be used for a wide variety of purposes such as model parameter verification, remote sensing algorithm validation, testing of new retrieval methods and future sensor studies. We show a specific implementation using the GEOS-5 model, the MODIS instrument and the MODIS Adaptive Processing System (MODAPS) Data Collection 5.1 operational remote sensing cloud algorithm processing chain (including the cloud mask, cloud top properties and cloud optical and microphysical properties products). We focus on clouds and cloud/aerosol interactions, because they are very important to model development and improvement.

1 Introduction

Accurate knowledge of cloud cover and cloud properties is important in model studies that involve Earth's radiative budget, climate prediction and numerical weather prediction. High clouds are observed to have a net warming effect on the atmosphere because of their low albedo and low temperature. Low clouds have a net cooling effect due to their high albedo and relatively small temperature contrast with the surface. Clouds and their interactions with aerosols are significant sources of uncertainty in climate prediction studies (IPCC, 2007). In addition, clouds continue to be the main

GMDD
6, 4105–4136, 2013

source of climate feedback uncertainty and hence climate sensitivity (e.g., Bony et al., 2006).

The Goddard Earth Observing System Version 5 (GEOS-5) earth system model is maintained by the Global Modeling and Assimilation Office (GMAO) at NASA Goddard Space Flight Center (GSFC). GEOS-5 contains components for atmospheric circulation and composition (including atmospheric data assimilation), ocean circulation and biogeochemistry, and land surface processes. Components and individual parameterizations within components are coupled under the Earth System Modeling Framework (ESMF, Hill et al., 2004). In addition to traditional meteorological parameters (winds, temperatures, etc., Rienecker et al., 2008), GEOS-5 includes modules representing the atmospheric composition, most notably aerosols (Colarco et al., 2010) and tropospheric/stratospheric chemical constituents (Pawson et al., 2008), and the impact of these constituents on the radiative processes of the atmosphere. GEOS-5 has a mature atmospheric data assimilation system that builds upon the Grid-point Statistical Interpolation (GSI) algorithm jointly developed with NCEP (Wu et al., 2002; Derber et al., 2003; Rienecker et al., 2008). The GSI solver was originally developed at NCEP as a unified 3-D-Var analysis system for supporting global and regional models. GSI includes all the in-situ and remotely sensed data used for operational weather prediction at NCEP. GEOS-5 also includes assimilation of Aerosol Optical Depth (AOD) observations from the MODerate resolution Imaging Spectroradiometer (MODIS) imager on the NASA Earth Observing System (EOS) *Terra* and *Aqua* spacecraft; an algorithm for assimilating cloud property information from measurements in the visible and infrared portions of the spectrum is currently under development (Norris and da Silva, 2013). While the GEOS-5 meteorological assimilation includes a wide variety of spaceborne sensor data, traditionally samples containing clouds are carefully screened out. The near real-time GEOS-5 data assimilation and forecasting system runs at a nominal horizontal resolution of 25 km with 72 vertical layers (Rienecker et al., 2008; Molod et al., 2012).

GMDD
6, 4105–4136, 2013

The MODIS instrument (Barnes et al., 1998) is a passive imager, producing a wide variety of remotely sensed data products for land, ocean and atmosphere disciplines from 36 spectral channels. Data Collection 5.1 processing includes algorithms for retrieving cloud cover amount (Ackerman et al., 2006; Frey et al., 2008), cloud top properties such as cloud top pressure and temperature (Menzel et al., 2008) and cloud optical and microphysical properties such as cloud optical thickness, cloud effective radius and cloud water path (Platnick et al., 2003; Wind et al., 2010; Zhang and Platnick, 2011; King et al., 2013).

In this paper we present a technique that brings together remote sensing methods and model-generated fields. We use MODIS geolocation data to sample GEOS-5 fields as if the MODIS instrument were flying over the model fields instead of the Earth surface. Once the sampling is complete, we generate equivalent sensor radiance data for the MODIS footprint. We then replace the contents of the 1 km, 500 m and 250 m resolution MODIS Level-1B (Xiong et al., 2006) radiance files with these simulated radiances and insert the resulting alternate data stream into the start of the MODIS Adaptive Processing System (MODAPS) operational algorithm processing chain for the atmosphere discipline cloud products mentioned above (product designation MOD06 and MYD06 for Terra and Aqua MODIS, respectively). The data stream is fully transparent to the system so that pixel-level (Level-2) retrievals can be aggregated through the same gridded (Level-3) $1^{\circ} \times 1^{\circ}$ code (Hubanks et al., 2006; King et al., 2003, 2013) used in MODAPS production (MOD08 and MYD08 for Terra and Aqua, respectively). There are many potential uses for the resulting Level-2 and Level-3 data. Level-3 model aggregations can be compared to archived MODIS Level-3 and GEOS-5 source data fields directly as a means of model validation and study of model biases that could exist. Level-2 data can be used to study some aspects of retrieval algorithm behavior and sensitivities since all retrievals are performed with known (prescribed) *truth*.

The equivalent sensor data framework has been developed with instrument flexibility in mind, so that by simple substitution of spectral response functions and data reader, the MODIS instrument can be replaced by other spaceborne or airborne sensors,

GMDD
6, 4105–4136, 2013

currently in operation or part of a future concept, and a different sensor data stream can be produced. Thus, identical products from different sensors or different retrieval algorithms for the same sensor can be compared and analyzed in a controlled environment, which can provide insight and lead to improvements in remote sensing algorithms.

This flexibility extends to model data as well. Any climate or weather prediction model fields can be used as long as a means of ingesting the necessary parameters is provided. Thus synthetic retrievals based on multiple models can be compared and analyzed using the same sensor interface in a controlled environment, leading to a consistent diagnostic toolset. Furthermore, this detailed simulation capability can function as a testbed for very fast simulators such as the Cloud Feedback Model Intercomparison Project (CFMIP) Observation Simulator Package (COSP) (Bodas-Salcedo et al., 2011) or the hyperspectral simulator of Feldman et al. (2011).

In Sect. 2 we describe the model–sensor interface using the GEOS-5 model and MODIS imager. Section 3 shows an example of simulation and retrieval of cloud properties on a sample Level-2 data granule. In Sect. 4 we elaborate on future directions for the software suite.

This paper is the first part in a series that will combine the software suite described in detail here with a variety of research applications.

2 Radiance simulations at scales smaller than the model's grid spacing

We start the process by selecting an area and time period of study. It can be as small as a few-pixel subsection of a single MODIS granule or as large as an entire year of MODIS data. The study size is only limited by availability of computing resources. As far as model itself is concerned, there is no need for actual MODIS data to be present, but we specifically want the actual MODIS radiances to be available, so that retrievals from simulated and actual radiances can be compared directly. Similarities and differences in those retrievals can be analyzed and results applied on a variety of levels in order to improve both the model and the sensor retrieval algorithm.

GMDD
6, 4105–4136, 2013

For simplicity's sake in all subsequent references and illustrations the study area will be taken to be a standard 5 min MODIS data granule (approximate 2000 km in the along track direction by 2300 km). Once the granule is chosen, we proceed to choose model output files that bound the granule time. For example, for the granule at 02:00 UTC, we would select model output at 00:00 and 03:00 UTC. We use a MODIS standard geolocation file (MOD03 product) to define the spatial locations to sample the model fields. Solar and view angle information contained in the same MODIS geolocation file is also used in the simulation. For the examples shown in this paper we used the GEOS model v.5.7.2 output. A listing of specific GEOS-5 fields and products used in this suite is given in Table 1.

2.1 Surface albedo determination

In order to save on computational time we pre-determine surface albedo for the area of study. The surface albedo data comes from a variety of sources. Over ice-free ocean, MODIS geometry and model wind speed are used in a Cox–Munk ocean surface BRDF model (Cox and Munk, 1954) to produce cloud-free ocean surface reflectance. This model reflectance is calculated for four cardinal wind directions and then averaged into a lookup table (LUT), that is a function of wavelength, wind speed, solar and sensor zenith angles and relative azimuth angle. We do the calculation at three wind speeds of 3, 7 and 15 $m\,s^{-1}$. The LUT has 33 solar zenith values, 28 view zenith values and 37 relative azimuth values. We linearly interpolate as needed to obtain surface spectral albedo in the selected fifteen MODIS channels that have a shortwave reflective component. The MODIS channels used in the simulation and their central wavelengths are listed in Table 2. The ocean reflectance LUT contains data for channels 1–22 and 26 from the table. For the IR (infrared) channels that have no reflective component (27–36), a constant value of 0.015 is used. This value is based on the ocean surface emissivity value suggested by the MODIS cloud top properties algorithm.

Over land several methods are utilized to model the radiances for all MODIS channels. We use the MODIS land surface spectral albedo gap-filled dataset (Moody et al.,

GMDD
6, 4105–4136, 2013

2005, 2008) that has been updated for MODIS data Collection 6 and is derived from both Aqua and Terra data. In addition to providing 16 day time period averages every 8 days, the gap-filled albedo files are generated for each year separately (instead of aggregating all years together as was done previously). Further, spatial resolution has been improved to 1 km. These files are derived from the Collection 5 MCD42B product (Schaaf et al., 2011). This MODIS land surface albedo product is used directly for channels 1–7 and interpolated linearly to cover other MODIS spectral channels that fall within the 0.47–2.14 µm wavelength range. For wavelengths that are longer than 2.14 µm we use the surface emissivity dataset used in MODIS clear-sky profile retrievals (Seemann et al., 2008). For wavelengths shorter than 0.47 µm we use a seasonally averaged surface albedo database utilized by the MODIS deep-blue algorithm (Hsu et al., 2004) to obtain the albedo for the 0.41 µm channel and then interpolate for the 0.44 µm channel.

Over snow and sea ice we use the MODIS zonal snow/ice albedo dataset (Moody et al., 2007). The table lookup is determined by the MODIS pixel latitude, the International Geosphere–Biosphere Programme (IGBP) ecosystem type and snow/ice fractions from GEOS-5 FRSNO and FRSEAICE model fields.

The resulting surface albedo values are written out to file for each study area so that they can be referenced later for different simulation scenarios involving same area and time. A good example of such varying scenarios would be repeated experiments with or without the presence of aerosols.

2.2 Water vapor and other gaseous absorbers

After the surface albedo calculations are complete, we proceed to ingest the profiles of temperature, relative humidity, ozone concentration and atmospheric pressure. These profiles are downsampled to 27 atmospheric levels, as listed in Table 3, from the GEOS-5 native 72 vertical levels and sent to an atmospheric transmittance module that uses the correlated-k method (Kratz, 1995) to calculate weights and optical thicknesses for each atmospheric layer due to water vapor and other gaseous absorbers. In cases

GMDD
6, 4105–4136, 2013

where the surface is encountered at an altitude higher than 0 km, the profile is trimmed accordingly and the surface level is inserted as the last level to be used. We perform the vertical downsampling in order to save on the computational cost of the equivalent sensor radiance simulation step, with the bulk of downsampling occuring above the tropopause. We preserve finer vertical resolution in the troposphere. We find this to be permissible as radiance data stored in a MODIS L1B file has an accuracy to only the 5th decimal place and the uncertainty due to varying the number of vertical levels in the upper atmosphere is less than this data storage accuracy.

2.3 Generating cloud subcolumns

Sampling of model cloud-related fields to the MODIS pixel scale is not straightforward because cloud properties typically vary on scales not adequately resolved by the operational 0.25° GEOS-5 resolution. To sample cloud fields, 1 km MODIS pixels for each GEOS-5 gridcolumn are collected and the same number of pixel-like sub-columns is generated using a statistical model of sub-gridcolumn moisture variability. The general approach of Norris et al. (2008) is followed, namely using a parameterized probability density function (PDF) of total water content for each model layer and a Gaussian copula to correlate these PDFs in the vertical.

In this application, we use the skewed triangle PDF, which allows a simple inclusion of moisture variability skewness, a ubiquitous feature of atmospheric boundary layers. This PDF has a simple scalene form characterized by three parameters: a lower and upper bound and a mode. Under some circumstances, these three parameters can be directly diagnosed from the *layer mean* total water and condensate contents, q_t and q_c, and cloud fraction f, but in many cases some adjustments are necessary to f, and possibly q_c, to achieve consistency. The details of this calculation are beyond the scope of this paper and are described fully in Norris and da Silva (2013). Approximations must also be made in the case of clear or overcast layers, when the triangle is underdetermined.

GMDD
6, 4105–4136, 2013

For the Gaussian copula we use a correlation matrix with a fixed vertical decorrelation scale of 100 hPa, further modified by a multiplicative Riishojgaard (1998) flow-dependent correlation in total water that permits sharper decorrelation across inversion features. Further details are given in Norris and da Silva (2013). Once the correlation matrix is specified, the Gaussian copula correlated ranks of each of the gridcolumn's layers are easily generated (Norris et al., 2008) and then inverted with the cumulative distribution function (CDF) of each layer's skewed triangle distribution. The net result is an ensemble of subcolumns of total moisture content that sample the specified layer PDFs and have the specified vertical correlations and accompanying cloud and condensate overlap properties. The transformation of total moisture content to vapor, liquid water and ice contents assumes the vapor is capped at the GEOS-5 saturation vapor content and that the excess moisture is condensate, split between the phases using an ice fraction linear in temperature over the −35 to 0 °C range. It is these subcolumn condensates, combined with GEOS-5 diagnostic effective radii, that are used to evaluate subcolumn (or "pixel") liquid water and ice optical thicknesses for each layer. These are input to the MODIS radiance simulator code.

Note that the subcolumns generated in this way are horizontally independent (the independent column approximation or ICA), but are subsequently "clumped," or rearranged, to give horizontal spatial coherence, by using a horizontal Gaussian copula applied to condensed water path. This clumping acts to give the generated clouds a reasonable horizontal structure, such that the cloudy pixels in a gridcolumn are actually grouped into reasonable looking clouds, rather than being randomly distributed. This is important because the MODIS cloud optical and microphysical properties retrieval algorithm has some spatial variance tests for potentially partially-cloudy pixels, removing cloud edges by the so-called "clear-sky restoral" (Zhang and Platnick, 2011; Pincus et al., 2012). If clumping is not used, then individual points generated by ICA stand an exceptionally high chance of being eliminated by the clear sky restoral unless a model grid box has a nearly 100 % cloud fraction.

GMDD
6, 4105–4136, 2013

In practice, the clumping algorithm works as follows: a correlation matrix **C** is a generated between all pixels in a gridcolumn based on the distance between the actual pixels in the MODIS granule and assuming a nominal 5 km decorrelation length. If there are N pixels, **C** is an $N \times N$ matrix. This matrix is used by a Gaussian copula to generate N correlated ranks, which are subsequently used to sample (effectively, to re-order) a list of the N *simulated* pixels that has previously been sorted by column condensed water path (CWP). Because horizontally nearby pixels are more correlated by **C**, they will have a higher chance of having similar ranks, and therefore similar values of CWP. In this way the pixels are grouped together horizontally into coherent clouds. (Note that this clumping acts on subcolumns as a whole, and independent of the preexisting vertical correlations in the ICA subcolumns, so the clumping will work better for single cloud layers. For multilayer clouds, the layer that dominates the CWP will dominate the clumping.)

The sub-gridcolumn cloud generator described above is, of course, only one of many possible generators. A less complicated example, very much akin to the internal GEOS-5 treatment of cloud overlap, would be the following "homogeneous cloud, maximum-random overlap" generator: divide the atmosphere into pressure bands, e.g., low, middle and high bands, with interfaces at 700 and 400 hPa. Say we again wish to generate N subcolumns, $n = 1, \ldots, N$, for the gridcolumn. Then for each pressure band, generate a set of N uniform random numbers $\{r_n\}$ on [0,1], and for each model layer k falling within the band, assign cloudiness to layer k of subcolumn n if $r_n < f_k$, where f_k is that layer's cloud fraction. The fact that the *same* set $\{r_n\}$ is used for each layer k in the band enforces maximum cloud overlap *within* the band. But choosing independent sets of $\{r_n\}$ for each pressure band enforces random overlap *between* the bands. Finally, every subcolumn which is cloudy at layer k, shares the same homogeneous in-cloud condensate contents, $\frac{q_{(\mathrm{i,}j)k}}{f_k}$ where $q_{(\mathrm{i,l})k}$ are the layer mean condensate contents (i = ice, l = liquid water).

Note that this simple generator, as with the earlier more sophisticated generator, produces subcolumns of *condensate*. The specification of optical thicknesses from

GMDD
6, 4105–4136, 2013

condensate contents proceeds in the same way in both generators, as presented earlier. We emphasize this strategy because the reader should be very aware of the potential traps associated with using diagnostic layer cloud optical thicknesses *directly* from GCM (e.g., GEOS-5) output files. When using diagnostic layer cloud optical thicknesses directly, one must know whether they are in-cloud or "layer mean", and if in-cloud, for what cloud fraction. For example, for GEOS-5, the layer cloud optical thicknesses TAUCLW and TAUCLI are "in-cloud" values consistent with the maximum cloud fraction $f_{\max}$ of the layer's pressure band, *not* with the layer's actual cloud fraction f_k. This is because the GEOS-5 diagnostics internally dilute each layer's in-cloud cloud optical thickness (in an approximately radiatively-consistent manner) by stretching each layer's cloud fraction to its band's $f_{\max}$, in order that it may simply add the diluted layer "in-cloud cloud optical thicknesses" within a band to produce a "band in-cloud cloud optical depth", such as GEOS-5's "TAULOW". Because of this, the GEOS-5 diagnostic TAULOW, for example, can be regarded as the low-band in-cloud cloud optical thickness consistent with the model's low band cloud fraction CLDLOW. Similarly for TAUMID and TAUHGH. But note that one cannot simply add TAULOW, TAUMID and TAUHGH to get a column in-cloud optical thickness, because the actual column value depends on the overlap of these bands. Currently this overlap is random, and so we could express the column in-cloud optical thickness in terms of the sum over the 2^3 combinations of cloud/clear in the three bands, each with their respective fractions (e.g., a fraction CLDLOW · CLDMID · CLDHGH of the gridcolumn would have a column TAU of TAULOW + TAUMID + TAUHGH, a fraction CLDLOW · CLDMID · (1 – CLDHGH) would have a column TAU of TAULOW + TAUMID, etc.), and finally all normalized by the column cloud fraction CLDTOT = 1 – (1 – CLDLOW) · (1 – CLDMID) · (1 – CLDHGH).

Not surprisingly this gives

$$\text{TAUTOT} = \frac{\text{CLDLOW} \cdot \text{TAULOW} + \text{CLDMID} \cdot \text{TAUMID} + \text{CLDHGH} \cdot \text{TAUHGH}}{\text{CLDTOT}}$$

for the column in-cloud optical thickness, because we are assuming that we can average optical thickness (including zeros) in the horizontal, to get a layer mean optical

GMDD
6, 4105–4136, 2013

thickness. That assumption in itself is rather questionable, since cloud radiative properties are non-linear in optical thickness. It is therefore much more accurate to deal with radiative averages over subcolumn ensemble optical thicknesses, generated as we have described, than with "layer mean" or "band in-cloud" optical thicknesses directly.

The point we are ultimately making is that one cannot simply interpret the column consequences of model layer cloud diagnostics without a knowledge of the model's cloud overlap. This is why GEOS-5 now includes the COSP simulator suite to produce satellite observables with an inbuilt treatment of the model overlap.

2.4 Radiative transfer calculation

Now that we've collected all the necessary information about atmosphere and cloud layers, we begin the simulation process. The radiative transfer calculations were performed using the Discrete Ordinate Radiative Transfer (DISORT) code (Stamnes et al., 1988) with liquid water cloud phase function results from Mie calculations based on gamma distribution water droplet size distributions with an effective variance of 0.1 and bulk ice cloud phase models developed by Baum et al. (2005), both consistent with MOD06. We have experimented with a different number of computational streams in order to balance speed and desired accuracy. We found that only 16 streams were required to achieve the needed precision. Generally a large number of streams is required to accurately model the forward peak of the phase function and multiple scattering components. Initial calculations were done with 32 streams, however the execution time was rather prohibitive. We settled on 16 streams as a balance between execution time and precision as the difference in resulting equivalent sensor radiance between 32 and 16 stream simulations was less than 0.5 %. Also the forward peak is further truncated and use of the delta-fit method of Hu et al. (2000) can be considered sufficiently accurate, as described by Ding et al. (2009), for calculations where there is no stored accuracy limit such as the multilayer cloud simulations in Wind et al. (2010). As we pre-calculate the surface spectral albedos, we can save further time by calling DISORT in Lambertian mode with predetermined values. When we encounter cloud

GMDD
6, 4105–4136, 2013

subcolumns over the ocean, however, we must adjust the computed Cox–Munk surface albedo to compensate for the diffuse illumination that the presence of the cloud creates. A good value for the diffuse illumination albedo of a water surface is 0.05 (Platnick et al., 2003). We then linearly fit surface albedo as a function of cloud optical thickness, with full diffuse illumination at a total column cloud optical thickness of 3 and full Cox–Munk surface albedo at total column cloud optical thickness of 0.

3 Example retrievals

In this section we discuss two example results of radiance simulations and subsequent cloud property retrievals. We performed the simulation on the NASA Center for Climate Simulations (NCCS) Discover system using 12 Intel Westmere nodes with 12 cores each. The memory footprint of the software suite is very small, around 80 Mb peak usage, but the process is quite CPU-heavy. A full-resolution 1 km simulation using a full MODIS granule as a study area took about three and a half hours wall clock time to complete. Figure 1 shows resulting true-color RGB image of sample MODIS granule 2012 day 228 (15 August) at 12:00 UTC together with the true-color image of the actual MODIS granule before its channel data was replaced. Figure 1a shows the actual data acquired by Aqua MODIS and Fig. 1b shows the simulation result. GEOS-5 does not assimilate cloudy radiances and so there should be little expectation of a granule-level feature match. However, in this case the model does remarkably well with cloud placement. Bands of cloud over southern France are present and located properly, as are clouds over the northern Balkans and southern Asia Minor. The orographic clouds over Italy and Greece are also present, as are scattered clouds over the Sahara desert. There are some rather important differences between the model and the actual data, however, when it comes to cloud properties.

Figure 2 shows the results of running the Data Collection 5.1 operational retrieval chain on the resulting L1B file from model fields. Figure 2a shows the cloud thermodynamic phase, Fig. 2b the cloud top pressure, Fig. 2c the cloud optical thickness

GMDD
6, 4105–4136, 2013

and Fig. 2d the cloud effective radius retrieved with the VNSWIR (Visible, Near- or ShortWave InfraRed) and 2.1 µm channel combination. Figure 3 shows the actual Aqua MODIS retrieval for that same granule using identical panel arrangement.

The cloud field over the central Mediterranean is given improper vertical location by the model. The actual cloud field is retrieved as liquid water and is low cloud, with cloud top pressures of 800–900 mb. The model generates a thin cirrus cloud in that location with cloud top pressure of about 100 mb and of course ice thermodynamic phase. This has serious implications for outgoing radiation. The cloud field over Romania has a consistent phase, but the model indicates the cloud to be positioned somewhat higher in altitude than the observation and also significantly optically thicker than what is observed. The same is true for the cloud field over NW Turkey.

Figure 4 shows a cloud top pressure/cloud optical thickness joint histogram for the actual granule in Fig. 4a and simulated one in Fig. 4b. While in this comparison we are not necessarily looking for quantitative evaluation of model parameters, some things do tend to jump out. The actual MODIS granule has mostly low clouds that are moderately thick. The simulated granule on the other hand lacks low clouds almost entirely and instead produces thicker clouds at high altitude. The RGB images look very similar in this case, so the model is performing well on geographical cloud placement, but fails rather badly when it comes to proper cloud placement in altitude. This kind of disconnect can have some significant implications for Earth radiative budget calculations. It is one of our future goals to determine just how frequently such disconnects occur on the global scale.

Figures 5–8 show another simulation example, this time from Terra MODIS 2013 day 151 (31 May 2013) at 11:15 UTC. Figure 5 shows a true-color RGB image for simulated and actual MODIS granule together with the SWIR composite that allows user to visually estimate cloud thermodynamic phase. Ice clouds appear red in such image. We cannot show a SWIR composite for Aqua MODIS because of detector issues with the Aqua MODIS 1.6 µm channel that is needed to create the image. Figure 6 shows retrieval results for the simulated granule, Fig. 7 shows the actual Terra MODIS

GMDD
6, 4105–4136, 2013

granule retrievals. Figure 8 shows the joint histograms of cloud top pressure and cloud optical thickness. In this case there is actually reasonable agreement between sensor measurement and model cloud field representation both geographically and vertically. The model could have benefitted from producing somewhat more mid-level clouds, but overall the large convective system that dominates the scene is represented reasonably well, as are the broken clouds around it. In this case the MODIS operational cloud mask had some trouble detecting clouds in the sun glint region, but sun glint quite often can be a challenging area for retrieval algorithms.

The MODIS cloud top pressure retrieval is quite sensitive to ancillary atmospheric profile information (Menzel et al., 2008) and some of differences found in retrievals could be a result of different representations of the atmospheric profile by GEOS-5 and the NCEP Mesoscale Meteorological Model (MM5)-derived model profiles used during the MODIS retrieval.

Situations in which cloud optical thickness retrievals show significant differences tend to be more indicative of significant differences in cloud structure. Unlike cloud top pressure, cloud optical thickness retrievals have very little dependence on atmospheric profile information as there is very little atmospheric absorption in the 0.65 and 0.86 μm channels used to retrieve this quantity.

Cloud effective radius retrievals from the 2.1 μm channel depend somewhat on the atmospheric profile, but differences in that retrieval are also mainly due to differences in cloud microphysics present in the model and in the actual atmosphere. Retrieved cloud effective radius appears to be somewhat smaller overall for GEOS-5 data than for MODIS. Even though the clumped-ICA cloud formation method allows us to model some of the scene inhomogeneity normally encountered in actual MODIS data, the present implementation of the simulator does not admit sub-pixel-based effective radius artifacts such as ones appearing in MODIS (Zhang and Platnick, 2011). Also, GEOS-5 uses a simple diagnostic prescription of cloud effective radius that is loosely based on large scale observations of aerosol concentrations and their physical connection to cloud droplet size, and with the details being adapted based on consistency

GMDD
6, 4105–4136, 2013

with surface radiation budget estimates of shortwave cloud forcing. It is therefore not surprising that, in our preliminary results, there appears to be generally somewhat less variability in retrieved cloud effective radius from GEOS-5 than from real MODIS data.

4 Conclusions and future directions

We have developed a flexible software suite that allows us to interface model fields to operational satellite remote sensing retrieval algorithms. We have presented an example of its operation using the GEOS-5 model and MODIS instrument. We have demonstrated the power of this software in locating and quantifying problems with GEOS-5 cloud optical properties and cloud vertical distributions within the specific geographic and synoptic contexts observed in MODIS cloud granules.

In subsequent papers we will show a number of applications of this software. Our current plans include performing a number of large-scale simulation experiments using GEOS-5 nature run model data with resolutions as high as 7 km. We would like to examine impact of aerosols on cloud retrievals by performing simulations with and without model aerosol fields. Once operational cloud and aerosol retrieval algorithms are applied to such data, we may be able to quantify some aerosol effects on clouds and maybe even find some ways to retrieve aerosols above clouds.

We would also like to examine in detail the performance of COSP, the Cloud Feedback Model Intercomparison Project (CFMIP) Observation Simulator Package, which provides a means of simulating retrieved cloud properties from a variety of instruments, including MODIS, from model fields. The COSP package typically uses approximate, so-called "fast" simulators of cloud properties, whereas we are directly simulating radiances and performing the retrievals using actual operational retrieval codes. We thus have the ability to test the quality of the COSP fast simulators.

We also intend to apply this software suite to other remote sensing instruments, such as SEVIRI (Spinning Enhanced Visible Infrared Radiometer Imager) onboard the Meteosat Second Generation geostationary satellite series. SEVIRI has a sufficient

GMDD
6, 4105–4136, 2013

number of channels that MODIS-style cloud retrieval algorithms can be applied. SEVIRI acquires data in 15 min intervals at 3 km nadir resolution, thus giving fine temporal and spatial resolution for diurnal sampling. Applying the equivalent sensor radiance package to SEVIRI would allow us potentially to examine model cloud dynamics at a temporal resolution not offered by polar orbiting satellites.

We are confident that there are many other applications for this software that will be found in the future besides ones outlined above and that it will become a valuable tool for both the remote sensing and modeling communities.

The simulator code is available to users free of charge by contacting the authors and becoming a registered user of this software package so that any updates can be issued directly. There may be additional, wider distribution means in the future if the software shows signs of growing popularity.

Acknowledgements. The authors would like to thank the MODAPS members Georgios Britzolakis, Kurt Hoffman and Gang Ye for assisting us in processing simulated radiance files through the operational retrieval algorithm chain.

References

Ackerman, A., Strabala, K., Menzel, P., Frey, R., Moeller, C., Gumley, L., Baum, B., Seemann, S. W., and Zhang, H.: Discriminating clear-sky from cloud with MODIS Algorithm Theoretical Basis Document (MOD35), ATBD Reference Number: ATBD-MOD-06, available at: http://modis-atmos.gsfc.nasa.gov/reference_atbd.html (last access: 23 July 2013), 2006.

Barnes, W. L., Pagano, T. S., and Salomonson, V. V.: Prelaunch characteristics of the moderate resolution imaging spectroradiometer (MODIS) on EOS-AM1, IEEE Trans. Geosci. Remote Sens., 36, 1088–1100, 1998.

Baum, B. A., Heymsfield, A. J., Yang, P., and Bedka, S. T.: Bulk scattering models for the remote sensing of ice clouds, Part 1: Microphysical data and models, J. Appl. Meteor., 44, 1885–1895, 2005.

Bony, S., Colman, R., Kattsov, V. M., Allan, R. P., Bretherton, C. S., Dufresne, J. L., Hall, A., Hallegatte, S., Holland, M. M., Ingram, W., Randall, D. A., Soden, B. J., Tselioudis, G.,

GMDD
6, 4105–4136, 2013

and Webb, M. J.: How well do we understand and evaluate climate change feedback processes?, J. Climate, 19, 3445–3482, 2006.
Colarco, P., da Silva, A., Chin, M., and Diehl, T.: Online simulations of global aerosol distributions in the NASA GEOS-4 model and comparisons to satellite and ground-based aerosol optical depth, J. Geophys. Res., 115, D14207, doi:10.1029/2009JD012820, 2010.
Cox, C. and Munk, W.: Measurement of the roughness of the sea surface from photographs of the sun's glitter, J. Opt. Soc. Am., 44, 838–850, 1954.
Derber, J. C., Purser, R. J., Wu, W.-S., Treadon, R., Pondeca, M., Parrish, D., and Kleist, D.: Flow-dependent Jb in a global grid-point 3-D-Var, Proc. ECMWF annual seminar on recent developments in data assimilation for atmosphere and ocean, Reading, UK, 8–12 September 2003, 2003.
Ding, S., Xie, Y., Yang, P., Weng, F., Liu, Q., Baum, B., and Hu, Y.: Estimates of radiation over clouds and dust aerosols: optimized number of terms in phase function expansion. J. Quant. Spectrosc. Radiat. T., 110, 1190–1198, 2009.
Feldman, D. R., Algieri, C. A., Ong, J. R., and Collins, W. D.: CLARREO shortwave observing system simulation experiments of the twenty-first century: simulator design and implementation, J. Geophys. Res., 116, D10107, doi:10.1029/2010JD015350, 2011.
Frey, R. A., Ackerman, S. A., Liu, Y., Strabala, K. I., Zhang, H., Key, J., and Wang, X.: Cloud detection with MODIS, Part I: Recent improvements in the MODIS cloud mask, J. Tech., 25, 1057–1072, 2008.
Hill, C., DeLuca, C., Balaji, V., Suarez, M., and da Silva, A.: The architecture of the Earth System Modeling Framework, Comp. Sci. Engr., 6, 18–28, 2004.
Hsu, N. C., Tsay, S., King, M. D., and Herman, J. R.: Aerosol properties over bright-reflecting source regions, IEEE T. Geosci. Remote S., 42, 557–569, 2004.
Hu, Y.-X., Wielicki, B., Lin, B., Gibson, G., Tsay, S.-C., Stamnes, K., and Wong, T.: d-Fit: a fast and accurate treatment of particle scattering phase functions with weighted singular-value decomposition least-squares fitting, J. Quant. Spectrosc. Radiat. T., 65, 681–690, 2000.
Hubanks, A, P., King, M. D., Platnick, S. A., and Pincus, R. A.: MODIS Atmosphere L3 Gridded Product Algorithm Theoretical Basis Document, ATBD Reference Number: ATBD-MOD-30, available at: http://modis-atmos.gsfc.nasa.gov/MOD08_M3/atbd.html (last access: 23 July 2013), 2008.
Intergovernmental Panel on Climate Change (IPCC): Climate Change 2007: The Physical Science Basis, Contribution of Worrking Group I to the Fourth Assessment Report of the In-

GMDD
6, 4105–4136, 2013

tergovernmental Panel on Climate Change, edited by: Solomon, S., Qin, D., Manning, M., Chen, Z., Marquis, M., Averyt, K. B., Tignor, M., and Miller, H. L., Cambridge Univ. Press, Cambridge, UK, 2007.

King, M. D., Menzel, W. P., Kaufman, Y. J., Tanré, D., Gao, B. C., Platnick, S., Ackerman, S. A., Remer, L. A., Pincus, R., and Hubanks, P. A.: Cloud and aerosol properties, precipitable water, and profiles of temperature and humidity from MODIS, IEEE Trans. Geosci. Remote Sens., 41, 442–458, 2003.

King, M. D., Platnick, S., Menzel, W. P., Ackerman, S. A., and Hubanks, P. A.: Spatial and Temporal Distribution of Clouds Observed by MODIS onboard the Terra and Aqua Satellites, IEEE Trans. Geosci. Remote Sens. 57, 3826–3852, 2013

Kratz, D. P.: The correlated k-distribution technique as applied to the AVHRR channels, J. Quant. Spectrosc. Radiat. T., 53, 501–517, 1995.

Menzel, W. P., Frey, R., Zhang, H., Wylie, D., Moeller, C., Holz, R., Maddux, B., Baum, B. A., Strabala, K., and Gumley, L.: MODIS global cloud-top pressure and amount estimation: algorithm description and results, J. Appl. Meteor. Climatol., 47, 1175–1198, 2008.

Molod, A., Takacs, L., Suarez, M., Bacmeister, J., Song, I.-S., and Eichmann, A.: The GEOS-5 Atmospheric General Circulation Model: Mean Climate and Development from MERRA to Fortuna, Tech. Rep. S. Gl. Mod. Data Assim., 28, 2012.

Moody, E. G., King, M. D., Platnick, S., Schaaf, C. B., and Gao, F.: Spatially complete global spectral surface albedos: value-added datasets derived from Terra MODIS land products, IEEE T. Geosci. Remote S., 43, 144–158, 2005.

Moody, E. G., King, M. D., Schaaf, C. B., Hall, D. K., and Platnick, S.: Northern Hemisphere five-year average (2000–2004) spectral albedos of surfaces in the presence of snow: statistics computed from Terra MODIS land products, Remote Sens. Environ., 111, 337–345, 2007.

Moody, E. G., King, M. D., Schaaf, C. B., and Platnick, S.: MODIS-derived spatially complete surface albedo products: spatial and temporal pixel distribution and zonal averages. J. Appl. Meteor. Climatol., 47, 2879–2894, 2008.

Norris, P. M. and da Silva, A. M.: Monte Carlo Bayesian inference on a statistical model of sub-gridcolumn moisture variability using high-resolution cloud observations, Part I: Method, Q. J. R. Meteor. Soc., submitted, 2013.

Norris, P. M., Oreopoulos, L., Hou, A. Y., Tao, W.-K., and Zeng, X.: Representation of 3-D heterogeneous cloud fields using copulas: theory for water clouds, Q. J. R. Meteor. Soc. 134, 1843–1864, doi:10.1002/qj.321, 2008.

GMDD
6, 4105–4136, 2013

Pawson, S. R., Stolarski, S., Douglass, A. R., Newman, P. A., Nielsen, J. E., Frith, S. M., and Gupta, M. L.: Goddard Earth Observing System chemistry-climate model simulations of stratospheric ozone-temperature coupling between 1950 and 2005, J. Geophys. Res., 113, D12103, doi:10.1029/2007JD009511, 2008.

Platnick, S., King, M. D., Ackerman, S. A., Menzel, W. P., Baum, B. A., Riedi, J. C., and Frey, R. A.: The MODIS cloud products: algorithms and examples from Terra, IEEE Trans. Geosci. Remote Sens., 41, 459–473, 2003.

Rienecker, M. M., Suarez, M. J., Todling, R., Bacmeister, J., Takacs, L., Liu, H.-C., Gu, W., Sienkiewicz, M., Koster, R. D., Gelaro, R., Stajner, I., and Nielsen, J. E.: The GEOS-5 Data Assimilation System – Documentation of Versions 5.0.1, 5.1.0, and 5.2.0. Tech. Rep. S. Gl. Mod. Data Assim., 27, 2008.

Riishojgaard, L. P.: A direct way of specifying flow-dependent background error correlations for meteorological analysis systems, Tellus A, 50, 42–57, 1998.

Roberts, Y. L., Pilewskie, P., Kindel, B. C., Feldman, D. R., and Collins, W. D.: Quantitative comparison of the variability in observed and simulated shortwave reflectance, Atmos. Chem. Phys., 13, 3133–3147, doi:10.5194/acp-13-3133-2013, 2013.

Schaaf, C. L. B., Liu, J., Gao, F., and Strahler, A. H.: MODIS Albedo and Reflectance Anisotropy Products from Aqua and Terra, In Land Remote Sensing and Global Environmental Change: NASA's Earch Observing System and the Science of ASTER and MODIS, Remote Sensing and Digital Image Processing Series, edited by: Ramachandran, B., Justice, C., Abrams, M., Vol. 11, Springer-Cerlag, 873 pp., 2011.

Seemann, S. W., Borbas, E. E., Knuteson, R. O., Stephenson, G. R., and Huang, H.-L.: Development of a global infrared land surface emissivity database for application to clear sky sounding retrievals from multispectral satellite radiance measurements, J. Appl. Meteor. Climatol., 47, 108–123, 2008.

Stamnes, K., Tsay, S. C., Wiscombe, W., and Jayaweera, K.: Numerically stable algorithm for discrete-ordinate-method radiative transfer in multiple scattering and emitting layered media, Appl. Optics, 27, 2502–2509, 1988.

Wind, G., Platnick, S., King, M. D., Hubanks, P. A., Pavolonis, M. J., Heidinger, A. K., Yang, P., and Baum, B.: Multilayer cloud detection with the MODIS near-infrared water vapor absorption band, J. App. Met. Clim., 49, 2315–2333, 2010.

Wu, W. S., Purser, R. J., and Parrish, D. F.: Three-dimensional variational analysis with spatially inhomogeneous covariances, Mon. Weather Rev., 130, 2905–2916, 2002.

GMDD
6, 4105–4136, 2013

Xiong, X., Isaacman, A. T., and Barnes, W.: MODIS Level-1B Products, Earth Science Satellite Remote Sensing, Science and Instruments, vol. 1, 33–49, 2006.
Zhang, Z. and Platnick, S.: An assessment of differences between cloud effective particle radius for marine water clouds from three MODIS spectral bands, J. Geophys. Res., 116, D20215, doi:10.1029/2011JD016216, 2011.

GMDD
6, 4105–4136, 2013

Table 1. GEOS v.5.7.2 fields and products used in simulations.

Field Code	Description
U10M	U-component of wind speed at 10 m altitude
V10M	V-component of wind speed at 10 m altitude
FRSEAICE	Sea ice fraction
FRSNO	Snow fraction
PS	Surface pressure
T2M	Temperature at 2 m altitude
SLP	Mean sea-level pressure
QV2M	Specific humidity at 2 m altitude
O3	Ozone concentration profile
T	Temperature profile
DELP	Level pressure differential profile
RH	Relative humidity profile
CLOUD	Radiative cloud fraction profile
QLLS	Large scale cloud liquid water mixing ratio
QLAN	Anvil cloud liquid water mixing ratio
QILS	Large scale cloud ice mixing ratio
QIAN	Anvil cloud ice mixing ratio

GMDD
6, 4105–4136, 2013

Table 2. MODIS channels used in simulations.

Channel number	Central wavelength (μm)
1	0.65
2	0.86
3	0.47
4	0.55
5	1.24
6	1.63
7	2.13
8	0.41
9	0.44
17	0.91
18	0.94
19	0.94
20	3.7
22	3.9
26	1.38
27	6.2
28	7.3
29	8.5
31	11.0
32	12.0
33	13.2
34	13.4
35	13.8
36	14.2

GMDD
6, 4105–4136, 2013

Table 3. Vertical levels used in simulation.

Level number	Level altitude (km)
1	80
2	60
3	50
4	45
5	40
6	35
7	30
8	25
9	20
10	18
11	16
12	15
13	14
14	13
15	12
16	11
17	10
18	9
19	8
20	7
21	6
22	5
23	4
24	3
25	2
26	1
27	0

GMDD
6, 4105–4136, 2013

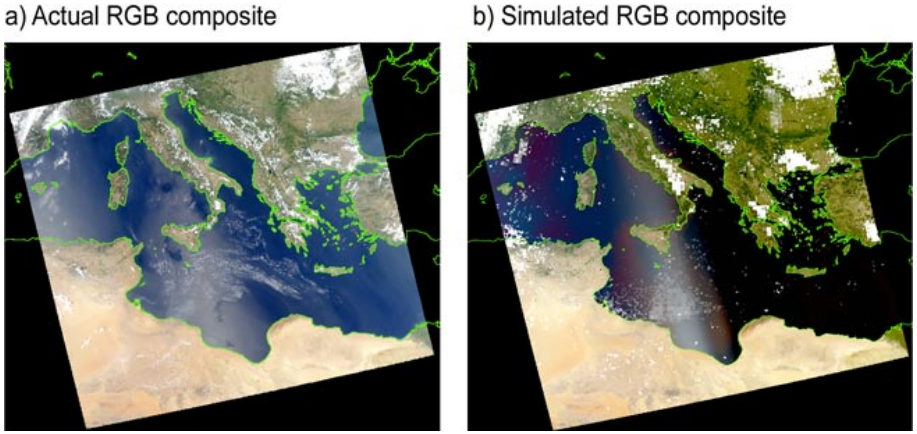

Fig. 1. Equivalent sensor radiance simulation together with an actual MODIS granule that was used as study area. Aqua MODIS granule 2012 day 228 at 12:00 UTC. GEOS-5 temporal fit between 12:00 UT and 18:00 UT, 15 August 2012. RGB (0.67, 0.55, 0.47 µm).

GMDD
6, 4105–4136, 2013

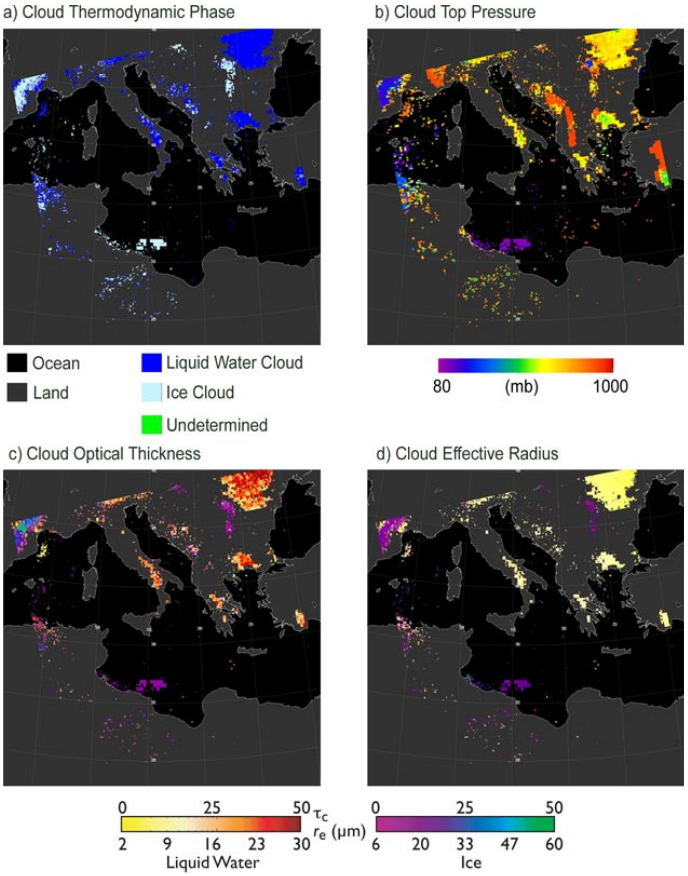

Fig. 2. Example cloud retrieval for simulated granule covered by Aqua MODIS 2012 day 288 12:00 UTC. Panel **(a)** is cloud thermodynamic phase, panel **(b)** is cloud top pressure, panel **(c)** is cloud optical thickness and panel **(d)** is cloud effective radius from the 0.86–2.1 μm band combination.

GMDD
6, 4105–4136, 2013

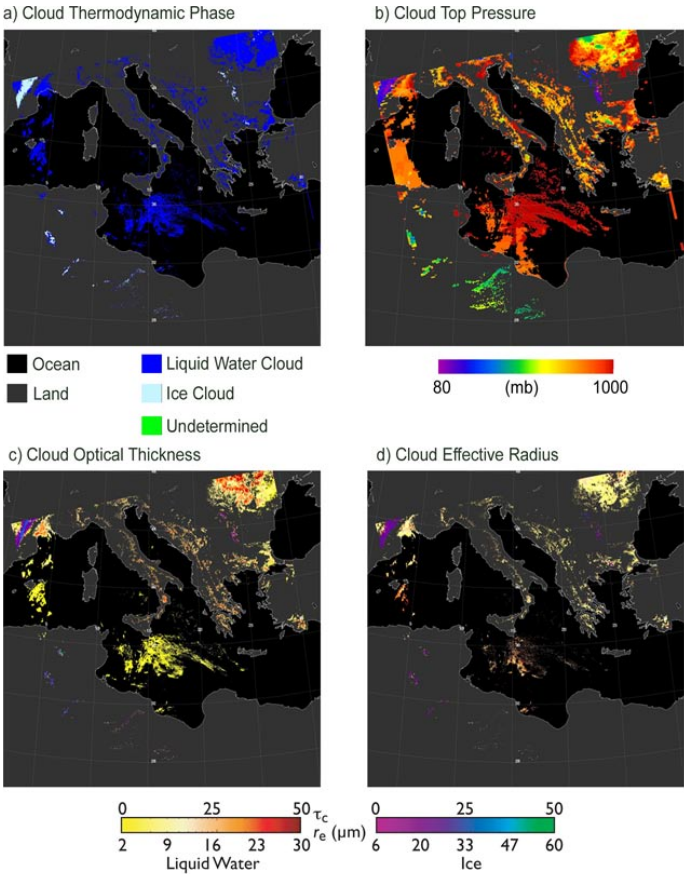

Fig. 3. Actual cloud retrieval for Aqua MODIS 2012 day 228 at 12:00 UTC. Panel **(a)** is cloud thermodynamic phase, panel **(b)** is cloud top pressure, panel **(c)** is cloud optical thickness and panel **(d)** is cloud effective radius from the 0.86–2.1 μm band combination.

GMDD
6, 4105–4136, 2013

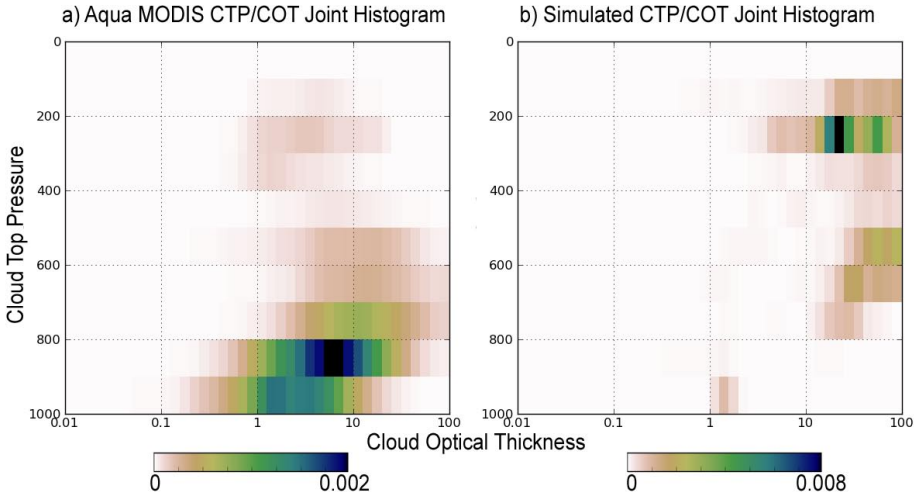

Fig. 4. Joint histograms of cloud optical thickness vs cloud top pressure for actual **(a)** and model-based **(b)** cloud fields covered by Aqua MODIS 2012 day 228 at 12:00 UTC.

GMDD
6, 4105–4136, 2013

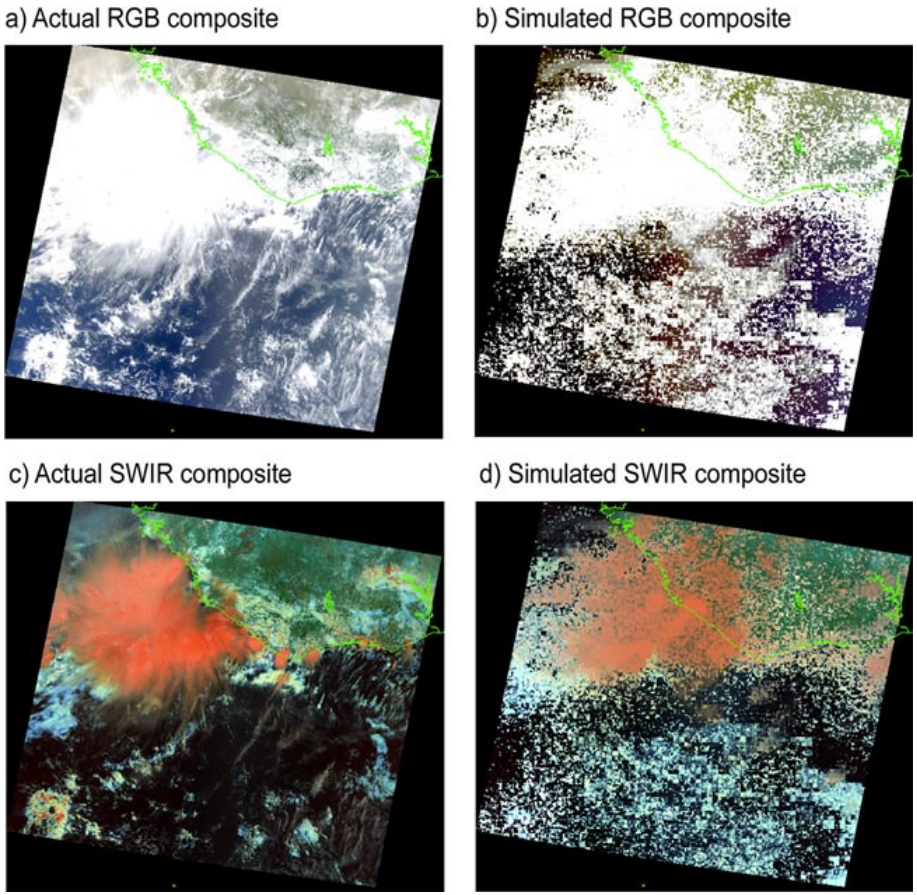

Fig. 5. Equivalent sensor radiance simulation together with an actual MODIS granule that was used as study area. Terra MODIS granule 2013 day 151 at 11:15 UTC. GEOS-5 temporal fit between 06:00 UT and 12:00 UT, 31 May 2013. RGB (0.67, 0.55, 0.47 µm), SWIR(0.86, 1.6, 2.1 µm).

GMDD
6, 4105–4136, 2013

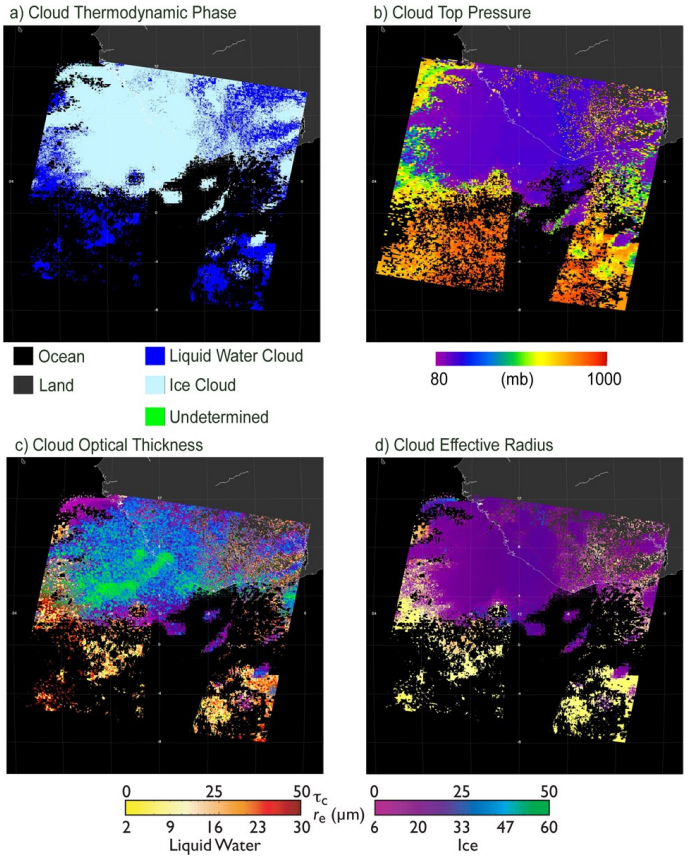

Fig. 6. Example cloud retrieval for simulated granule covered by Terra MODIS 2013 day 151 11:15 UTC. Panel **(a)** is cloud thermodynamic phase, panel **(b)** is cloud top pressure, panel **(c)** is cloud optical thickness and panel **(d)** is cloud effective radius from the 0.86–2.1 μm band combination.

GMDD
6, 4105–4136, 2013

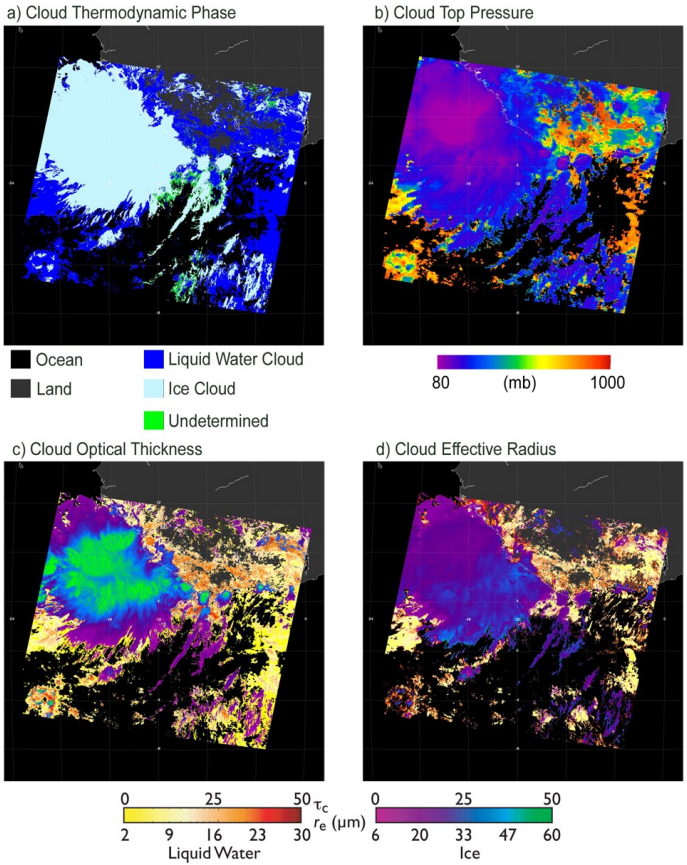

Fig. 7. Actual cloud retrieval for Terra MODIS 2013 day 151 at 11:15 UTC. Panel **(a)** is cloud thermodynamic phase, panel **(b)** is cloud top pressure, panel **(c)** is cloud optical thickness and panel **(d)** is cloud effective radius from the 0.86–2.1 μm band combination.

GMDD
6, 4105–4136, 2013

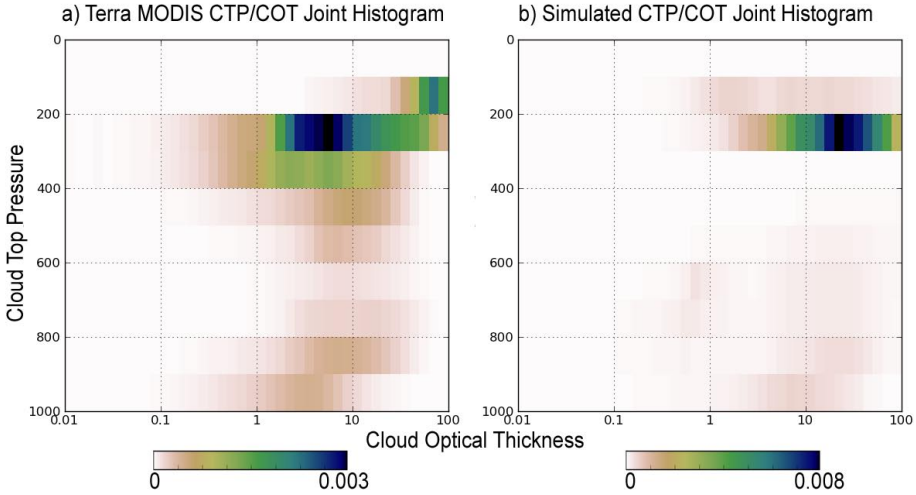

Fig. 8. Joint histograms of cloud optical thickness vs cloud top pressure for actual **(a)** and model-based **(b)** cloud fields covered by Terra MODIS 2013 day 151 at 11:15 UTC.

GMDD
6, 4105–4136, 2013

MODIS Cloud retrieval simulator and applications

G. Wind et al.